Research Article Vol. 30, No. 6 / 14 Mar 2022 / Optics Express 8876
Optics EXPRESS

To focus-match or not to focus-match inverse spatially offset Raman spectroscopy: a question of light penetration

GEORGINA E. SHILLITO,[1] LEWIS MCMILLAN,[1] GRAHAM D. BRUCE,[1,*] AND KISHAN DHOLAKIA[1,2,3]

[1]SUPA School of Physics and Astronomy, University of St Andrews, North Haugh, St Andrews KY16 9SS, United Kingdom
[2]Department of Physics, College of Science, Yonsei University, Seoul 03722, Republic of Korea
[3]School of Biological Sciences, The University of Adelaide, Adelaide, South Australia, Australia
*gdb2@st-andrews.ac.uk

Abstract: The ability to identify the contents of a sealed container, without the need to extract a sample, is desirable in applications ranging from forensics to product quality control. One technique suited to this is inverse spatially offset Raman spectroscopy (ISORS) which illuminates a sample of interest with an annular beam of light and collects Raman scattering from the center of the ring, thereby retrieving the chemical signature of the contents while suppressing signal from the container. Here we explore in detail the relative benefits of a recently developed variant of ISORS, called focus-matched ISORS. In this variant, the Fourier relationship between the annular beam and a tightly focused Bessel beam is exploited to focus the excitation light inside the sample and to match the focal point of excitation and collection optics to increase the signal from the contents without compromising the suppression of the container signal. Using a flexible experimental setup which can realize both traditional and focus-matched ISORS, and Monte-Carlo simulations, we elucidate the relative advantages of the two techniques for a range of optical properties of sample and container.

1. Introduction

The use of Raman spectroscopy to perform in-situ measurements without removing a sample from its original container allows for precise chemical analysis without sample contamination or loss of value. It has therefore seen increasing application in quality assessment, product discrimination, and anti-counterfeiting in food and drink [1–3], as well as forensic [4,5] and security applications [6,7]. Raman spectroscopy is often conventionally performed in a back-scattering, 180° geometry, where the incident and scattered radiation are delivered and collected along the same optical path. For a sample which is contained behind an external layer, this method typically results in a bias towards signal generated from the surface. Therefore, a thick and/or highly Raman active or fluorescent barrier material can interfere with or prevent the collection of a Raman signature from the contents.

Raman spectra of the contents can be better isolated using a technique known as spatially offset Raman spectroscopy (SORS) [8,9]. Unlike conventional Raman spectroscopy, SORS involves a lateral, physical separation of the illumination and collection sources, Δs, such that the scattered photons are collected at a distance away from the incident beam. Increasing the value of Δs allows spectra of the sample to be obtained at increasing depths. Pure sample spectra can be obtained through scaled subtraction of the spectrum acquired where the collection and excitation points overlap, i.e., $\Delta s = 0$, but in general, the signal intensity from the contents is much lower

#451496 https://doi.org/10.1364/OE.451496
Journal © 2022 Received 17 Dec 2021; revised 9 Feb 2022; accepted 10 Feb 2022; published 2 Mar 2022

Optics EXPRESS

for SORS than for conventional Raman spectroscopy. Suppression of the container signal can be further improved by shifting the collection point inside the sample [10,11]. SORS has been utilized to measure liquid and solid samples through transparent, as well as opaque containers [2,7,8,12–16].

A similar technique, known as inverse-SORS (ISORS) utilizes an annular beam to illuminate the sample and the scattered light is measured from the center of the ring, such that the offset distance corresponds to the ring radius [17]. Typically, a diverging annular beam is formed using an axicon and the ring radius is varied by changing the axicon position. ISORS can give greater signal intensities compared to SORS [17,18], but still with significantly lower signal intensity than is achievable in conventional Raman spectroscopy. The effectiveness of this technique for interrogating samples at depth has been demonstrated for a range of media, including the detection of pharmaceuticals within plastic containers, tablets and envelopes [19] as well as the detection of muscle tissue contained within paraffin blocks [20] and transcutaneous bone detection [18].

Recently, we introduced an axicon-based, back-scattering geometry to obtain Raman spectra of whisky samples through their original glass bottles [21]. Like ISORS, this geometry illuminates the sample with an annular beam, and collects scattered light through the dark center of this beam, to selectively suppress signal from the glass. However, this geometry focusses the annular beam to take advantage of the Fourier relationship between the annular beam formed by an axicon and a Bessel beam, creating an intense focus *inside* the sample of interest. Similarly to conventional Raman spectroscopy, the Raman scattered light is collected from this excitation focal point to maximize the total Raman signal collected. In this work, we refer to this geometry as *focus-matched ISORS*.

While focus-matched ISORS has been demonstrated for alcoholic beverages in glass bottles, what remains unclear is how the relative benefits of focus-matched and traditional ISORS are influenced by the optical properties of the sample under investigation. Here, we answer this question using a combination of a reconfigurable experimental set-up and Monte Carlo Radiation Transfer (MCRT) simulations of the light propagation [22–24]. We establish that the focused-matched ISORS geometry increases the signal retrieved from the contents while achieving a comparable suppression of the container signal to traditional ISORS for samples with a high optical penetration depth, and show that for samples with low penetration depths the two techniques offer comparable performance.

2. Materials and methods

2.1. Equipment

The experiments were conducted with the arrangements shown in Fig. 1. A tunable Ti:sapphire laser (Spectra-Physics 3900s) was used to excite the sample with 785 nm light, with a power of approximately 100 mW at the sample surface. The laser is sent through a single mode optical fiber (SF), collimated with a plano-convex lens (C), passed through a line filter (LF) into an axicon lens (Ax, Thorlabs Ax255-B, $\alpha = 10°$) forming a Bessel beam. The remaining lenses (L_{1a}, L_{2a}, L_{3a}, L_{1b}, L_{2b} and L_{3b}) were achromatic doublets.

2.2. Flexible ISORS setup

For comparative measurements between traditional ISORS, focus-matched ISORS and conventional Raman Spectroscopy (reported in Section 3.1 below), a flexible ISORS configuration was used (Fig. 1(a)). The annular beam passes through another lens (L_{1a}, $f = 60$ mm) which can be moved in conjunction with the axicon lens (Ax) at a fixed separation distance of 133 mm. This changes the axial location at which the Bessel beam forms, as indicated by the arrows in Fig. 1(a). The annular beam is reflected by a dichroic mirror (DM) and onto the sample. The Raman

Optics EXPRESS

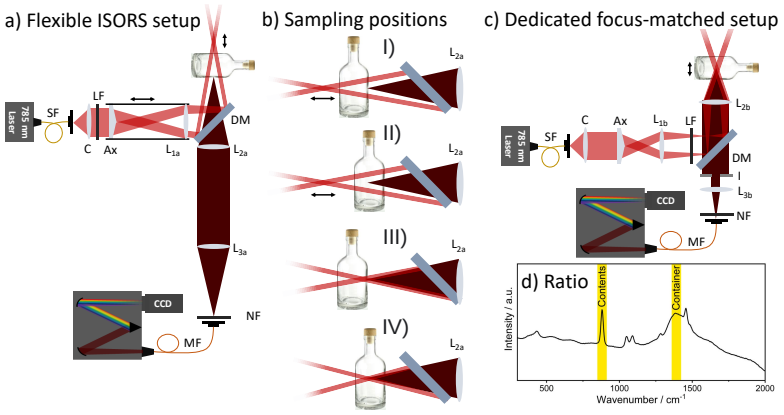

Fig. 1. Experimental geometries. a) Flexible ISORS configuration, where the axicon Ax and first lens L_{1a} can be moved as a unit along the optical cage, varying the position of the second Bessel beam and hence the ring radius on the sample surface. Signal can be collected from the container surface or interior, by changing the position of the sample. b) Illustrations of the sampling positions used; I) surface collection ISORS, II) inside collection ISORS, III) conventional Raman spectroscopy, IV) focus-matched ISORS. c) A separate focus-matched only geometry where the excitation and collection pathways always overlap, which is discussed in Section 3.3. d) Illustrative ISORS spectrum of whisky in a glass bottle showing the presence of signal from both the contents (ethanol) and container (glass). The intensities of the strongest ethanol peak (880 cm^{-1}) and the strongest glass peak (1381 cm^{-1}) are used to calculate the container-to-contents ratio.

scattering is collected in a back-scattering configuration, with collection optics (L_{2a}, $f = 80$ mm and L_{3a}, $f = 80$ mm) forming a standard 4-f system, passed through a notch filter (NF) to exclude Rayleigh scattering and focused into a multi-mode collection fiber (MF, 200 µm core diameter, 0.22 NA). This is passed through a spectrometer (Shamrock SR-303i, Andor Technology) onto a thermoelectrically cooled CCD camera (Newton, Andor Technology).

As shown in Fig. 1(b), the collection position was either directly on the surface of the sample (I and III) or at a fixed distance inside the sample, beyond the container surface (II and IV). The collection point was altered by adjusting the position of the sample. The translation of the Ax-L_{1a} pair varies the axial position of the Bessel beam, and therefore the ring radius on the sample surface. In any configuration where the collection and excitation foci are not overlapped, the system could be described as traditional ISORS – although this name is usually associated with the collection focus being on the container surface as in Fig. 1(b) I) rather than inside the container as in Fig. 1(b) II). Importantly, there are two special cases when the collection and excitation foci are overlapped: a conventional Raman geometry (where the collection and excitation occur from a common spot, i.e. $\Delta s = 0$ mm, on the sample surface), and the focus-matched ISORS configuration (where the collection and excitation points overlap inside the sample), shown in Fig. 1(b) III) and IV), respectively.

2.3. *Dedicated focus-matched ISORS setup*

For investigations into the key experimental parameters for an optimized focus-matched ISORS (section 3.3 below), a more compact experimental geometry was used (Fig. 1(c)). Here, the excitation and collection always overlap (meaning only configurations shown in Fig. 1(b) III and IV can be obtained), so the ring radius and hence the focus and collection point are varied through

Optics EXPRESS

movement of the sample only. The axicon and L_{1b} ($f = 100$ mm) are in a fixed position 113 mm apart. The excitation and collection geometries overlap through a lens (L_{2b}, $f = 40$ mm) placed after the dichroic mirror (DM), which forms part of the 4-f collection system (L_{3b}, $f = 50$ mm). An iris (I) with a diameter of ~10 mm, is placed between L_{2b} and L_{3b} which functions to help exclude Raman signal from the sample surface, such that the majority of photons are collected from inside the ring. The use of different lens combinations in the focus-matched system was explored, with further details found in the Supporting Information (Figure S1).

2.4. Materials and acquisition parameters

We investigated the benefits of the focus-matched approach in a range of samples with varying absorption and scattering properties. Samples measured experimentally range from almost-transparent to highly opaque. These include whiskies in their original clear glass bottles with a diameter of 70 or 35 mm as well as a white, opaque plastic bottle made of high-density polyethylene (HDPE) filled with paracetamol tablets available over-the-counter. In addition, a white Lego block, made from 5 mm thick acrylonitrile butadiene styrene (ABS), concealing crushed paracetamol tablets was also measured. Spectra were obtained using a 2 s exposure time and 30 accumulations, with three spectra obtained for each measurement. To quantify the contents or container signal, we use the height of the largest peak in the relevant Raman spectrum (880 cm^{-1} corresponding to the ethanol content of alcohol, 858 cm^{-1} for paracetamol, 1381 cm^{-1} for glass, 1063 cm^{-1} for HDPE, 1003 cm^{-1} for ABS plastic). There is only negligible contribution to these peak heights from the other materials, for each combination in use in this work. An example of the combined glass and alcohol spectrum can be seen in Fig. 1(d). The container-to-contents ratio, with intensities measured from the baseline, was calculated. Here a *decrease* in value corresponds to an *increase* in relative contribution of the contents signal. In certain situations (*vide infra*) the container signal is excluded entirely, leading to a ratio of zero. Error bars represent the standard deviation between three repeat measurements where the sample was removed and replaced.

All measurements had a dark (CCD slit closed) background correction. The spectra were individually processed, and the average container-to-contents ratios and signal intensities of triplicate measurements were used in the analysis. For the plastic containers, a baseline subtraction using an adaptive baseline tool was performed to remove a portion of the background to better compare relative Raman intensities of the container and contents bands. In the case of the alcohols in glass bottles no baseline subtraction was performed. The ISORS spectra are presented without any scaled subtraction of a container reference (i.e., $\Delta s = 0$) spectrum for all sample types. Signal-to-noise (SNR) calculations were performed using the method reported by McCreery [25]. The SNR was calculated by taking the mean peak height above the baseline divided by σ. The value of σ was determined by subtraction of two successive spectra and taking the standard deviation of the resulting noise spectrum in the peak region, divided by $\sqrt{2}$. Spectral processing was performed using SpectraGryph software [26].

2.5. Computational analysis

To establish the range of samples for which the focus-matched geometry offers an advantage, and in particular to investigate the parameter range between experimentally measured samples in a controllable way, we performed numerical simulations of the light propagation inside the media of interest. As the interaction of light and turbid media is not easily elucidated, we employ simulations of light transport using the MCRT method to shine light on this problem. MCRT is a stochastic method that uses interaction probabilities and random numbers to fully simulate the propagation of light though various media. We employ it in this work to determine the evolution of the excitation intensity within the container, and thus determine in what types of media the focus-matched ISORS geometry excels.

Optics EXPRESS

The MCRT code we used in this work was originally developed for simulating light transport in dusty galaxies [24], and has since been adapted for use in medical [22], and biophotonics [23] applications. Here, we specifically use the newly-developed signedMCRT method, which allows the accurate modelling of arbitrary curved surfaces [27]. Light impinges on a semi-infinite slab, whose optical properties (specifically the scattering and absorption coefficients, refractive index and the anisotropic scattering parameter) can be set such that they mimic different media of interest. The medium is divided into $200 \times 200 \times 200$ voxels giving a resolution of 0.15 mm. The propagation of 10^7 photons is simulated, with an initial position- and direction-distribution chosen to match the experimental geometry. The number of voxels gives sufficient resolution for the problem, and the number of photons simulated gives an adequate signal to noise ratio for the mean intensity. The trajectory of each photon is traced to the desired focal plane, as is the backward propagation of photons to the plane of the collection fiber. To parameterize the effect of the medium properties, we compare the light intensity reaching the fiber plane (taking only photons within the central 200 μm and an angle of incidence within the typical numerical aperture (0.22) to mimic the fiber collection) from photons originating both within the sample of interest and from the container. Simulations were fully parallelized and run on an AMD Ryzen 9 3950X 16-Core Processor and took between 0.5 and 3.0 minutes per sample.

3. Results and discussion

3.1. ISORS optimization in opaque and transparent samples

In this section we present a set of comparative measurements between conventional Raman spectroscopy, traditional ISORS, and focus-matched ISORS. All measurements are performed using the flexible setup shown in Fig. 1(a), by varying the relative axial positions of the container, the excitation beam and the collection optics, as detailed in Section 2.2. This allows us independence to vary both the collection point and the radius of the ring of light on the front surface of the container. In Figs. 2 and 3, we present the effect of the experimental geometry on the contents signal strength, the container signal strength, and the container-to-contents ratio. Figure 2 outlines investigations of samples of whisky in 70 mm-diameter colorless glass bottles, while Fig. 3 details investigations of paracetamol tablets in an opaque, white, 40 mm diameter HDPE bottle.

As mentioned previously, typical ISORS measurements are performed by scaled subtraction of a zero-offset spectrum from that obtained at a specific radial offset. The zero-offset measurement is performed when the annular beam is focused to form a spot on the sample's surface. When the collection point is also on the sample's surface, overlapping with the excitation, the resulting geometry is analogous to a conventional Raman configuration, such that the majority of the signal contribution is due to the container. In general, the greater the radial offset distance, the greater the relative contribution of photons from sub-surface contents to the spectrum [28]. Such a behavior was reported by Matousek for a two-layer system of trans-stilbene powder contained behind a layer of PMMA powder, where increasing the ring radius from 0.9 to 3.8 mm reduced the surface layer signal by a factor of ~13, but was also accompanied by a decrease in overall signal strength [17].

Using the flexible ISORS geometry to vary the ring radius while fixing the collection focus on the surface of the bottle (see Fig. 2(d) I for a pictorial representation), the general trend of ISORS outlined above was reproduced for whisky in a glass bottle (blue points in Fig. 2(a)). When the excitation focal point overlaps with the collection focal point (vertical line III), a conventional Raman spectroscopy geometry is realized, as represented in Fig. 2(d) III. This maximizes both the signal from the contents and the container. However, as shown in Fig. 2(b), while this geometry maximizes the contents signal, the enhancement of the container signal is even higher, leading to a container-to-contents ratio of ~60. Increasing the ring radius causes both contents and

Optics EXPRESS

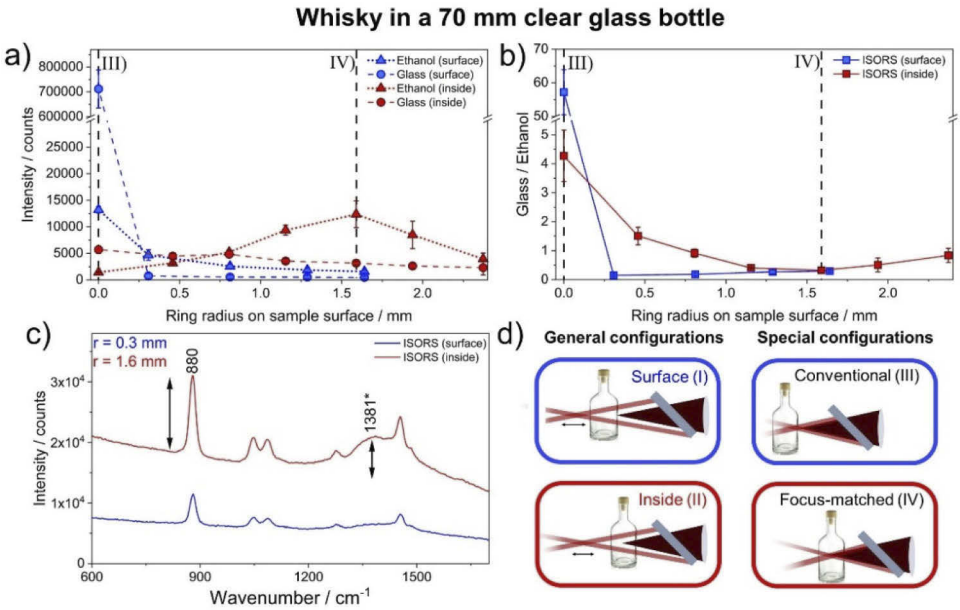

Fig. 2. Variations of Raman spectra obtained from whisky in a 70 mm glass bottle as a function of ring radius on the container surface, obtained using the flexible ISORS setup of Fig. 1(a). For all panels, blue (red) data points correspond to a collection focal point on the surface (inside) of the container – i.e., the configurations in d) I and d) II respectively. A conventional Raman spectroscopy geometry is realized at the vertical dashed line (III) for surface collection, and focus-matched ISORS is realized at vertical line (IV) for the internal collection, as illustrated in the corresponding diagrams in d) III and d) IV. a) Intensities of highest spectral features of the glass (circles) and the alcohol (triangles) as a function of ring radius. For both collection points, the alcohol signal intensity is highest when the excitation focus overlaps with the collection point (dashed vertical lines – III for blue, IV for red). However, for surface collection this is dominated by a contribution from the glass signal which is 60 times *stronger* than the contents signal. For collection inside the bottle the glass intensity is 19 times *weaker* than the contents signal. b) Container-to-contents ratios as a function of ring radius. For surface collection, a minimal value of container-to-contents ratio is obtained at distances close to the surface. For collection at depth, the minimal container-to-contents ratio is obtained at the focus-matched ISORS configuration. c) Representative spectra obtained at the point of lowest container-to-contents ratio (r = 0.3 mm for surface collection, r = 1.6 mm for inside collection). The alcohol peak highlighted at 880 cm^{-1} and glass peak highlighted at 1381 cm^{-1} are the strongest spectral features, and it is the height of these peaks which is plotted in panel (a), and their ratio is plotted in panel (b). d) Illustrative representation of the sampling configurations.

container signal to drop (Fig. 2(a)), but the container signal is suppressed more strongly, so that increasing the ring radius to 0.3 mm gives a container-to-contents ratio of 0.15.

When the collection point is moved to 22 mm inside the bottle (red points in Fig. 2, configuration shown in Fig. 2(d) II), an entirely different trend can be observed. While the glass signal once again falls as the ring radius is increased, the signal from the ethanol now exhibits a non-monotonic variation with ring radius (Fig. 2(a)). In particular, the signal from the contents reaches a peak value when the collection focal point and the excitation focal point overlap (vertical line IV). The configuration which creates this peak is the focus-matched ISORS geometry, which is pictorially

Optics EXPRESS

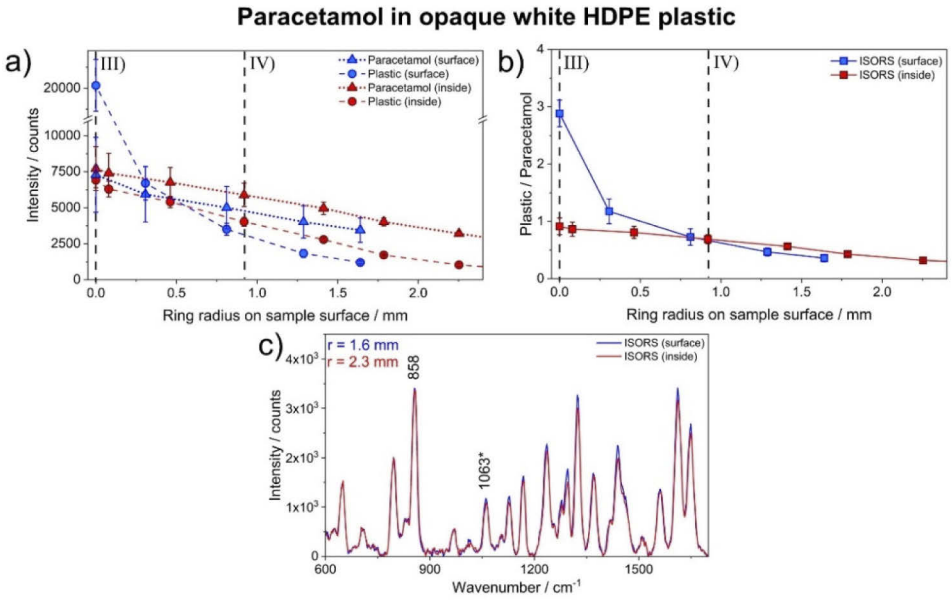

Fig. 3. Variations of Raman spectra obtained from paracetamol in a HDPE plastic bottle as a function of ring radius on the container surface, obtained using the flexible ISORS setup of Fig. 1(a). Panels a-c) show the same representations as in Fig. 2(a)-(c)). Contents and container bands are measured at 858 and 1063 cm^{-1}, respectively. Container reference band shown by *. Unlike the alcohol-glass combination, there is no measurable increase in contents signal for paracetamol in plastic, in the focus-matched ISORS configuration.

represented in Fig. 2(d) IV. As shown in Fig. 2(b), a parabolic-like behavior of the container-to-contents ratio as a function of ring radius is observed, where the best container-to-contents ratio of 0.32 is obtained with a radius of 1.6 mm. While the suppression of the glass is slightly poorer than with the surface collection, there is a considerable improvement made in the overall spectral intensity, particularly that of the ethanol signal, being approximately 3x that obtained at the best glass suppression point with surface collection (see Fig. 2(c) for example spectra obtained at the locations of minimum container-to-contents ratio for each collection point). This increase in signal strength is accompanied by a similar improvement in the SNR of the 880 cm^{-1} band, from SNR = 70 in the traditional ISORS geometry to SNR = 180 in the focus-matched ISORS geometry. This focus-matched geometry simultaneously realizes the advantages of both conventional Raman spectroscopy and conventional ISORS, achieving a signal intensity from the contents which is comparable to that achieved with conventional Raman, with an ability to suppress the surface signal which is comparable to that achieved with ISORS (see also Figure S2).

The same experiment was repeated with paracetamol tablets inside an opaque white HDPE bottle. As shown in Fig. 3 for both surface (blue points) and internal (red points) collection, an increase of the ring radius decreases the plastic-to-paracetamol ratio (measured at 1063 and 858 cm^{-1} respectively, due to the high intensities of these bands), corresponding to a relative increase in signal contribution from paracetamol. This is recognizable as typical ISORS behavior. Interestingly, when the excitation beam is focused on the surface, an improvement in the container-to-contents ratio without sacrifice in contents signal is obtained by applying an axial offset [10,11], i.e. moving the collection point 15mm inside the bottle (shown by the change in container-to-contents ratio along the vertical line III in Fig. 3(b)). For this internal

Optics EXPRESS

collection point, the conditions for a focus-matched configuration are achieved at a ring radius of 0.9 mm (vertical line IV). However, unlike with the whisky samples, no notable change in the container-to-contents ratio is seen at this point. Indeed, the optimal spectra obtained for each collection point are almost indistinguishable, as shown in Fig. 3(c). This is also the case for a Lego block concealing a layer of paracetamol powder - further details can be found in Figure S3. To better understand why the focus-matched geometry does not outperform typical ISORS behavior in more highly scattering media, we undertook a numerical study using MCRT to simulate the propagation of light in the various scattering media.

3.2. Role of sample optical properties

To investigate under which conditions the use of the novel focus-matched ISORS geometry is advantageous, we numerically modelled the propagation of the beam in a semi-infinite slab with variable scattering and absorption properties, a fixed refractive index (1.3) and anisotropy g value (0.7) [29] and propagated an annular beam into a focus at 1.55 cm depth. Figure 4 shows the results of these MCRT simulations.

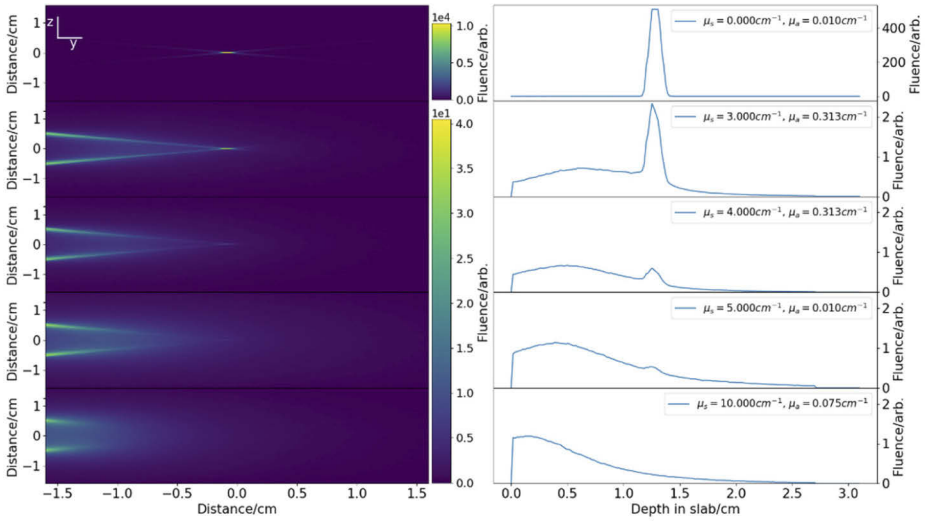

Fig. 4. Penetration of excitation light into samples with differing optical properties. Left panels: Cross section of intensity on the y-z plane at x = 0 for a range of optical properties, $\mu_s = [0, 10]$ cm^{-1} $\mu_a = [0.01, 0.313]$ cm^{-1}. As the optical properties are increased, we see that the annular beam no longer focuses to a point. Right panels: Average intensity of the 9 pixels around the line x = z = 0. As we increase the scattering and absorption coefficients of the slab, ballistic photons are prevented from reaching the focal distance (peaks in top 3 panels). At higher scattering coefficients, scattering dominates and produces the characteristic scattering curve near the surface of the slab.

The Raman signal from the contents will be directly proportional to the peak intensity in the medium. Figure 4 shows the peak intensity along the central axis of the beam, for varying scattering μ_s and absorption coefficients μ_a. The optical penetration depth $\delta = (\sqrt{3\mu_a(\mu_a + \mu_s(1-g))})^{-1}$ is a useful parameter to consider the combined effect of these two phenomena, where g is the scattering anisotropy [30]. In the high-penetration limit (no scattering or absorption), the intensity shows a large peak at the focal location of the annular beam. The peaks at ~1.4 cm correspond to the offset focal depth due to the refractive index at the boundary and comes from ballistic photons which are unscattered by the media. As the penetration depth is reduced, the height of the peak is lowered whilst a second broader peak appears at shallower depth. This shallower

Optics EXPRESS

peak is the peak of the scattered photons as opposed to the ballistic photons. Figure 4 shows clearly that as the penetration depth is lowered the ballistic peak becomes negligible compared to that of the scattered peak. The focus-matched ISORS geometry is critically dependent on an abundance of ballistic photons, i.e., photons that undergo little to no scattering, to produce the strong signal from the contents. Indeed, this is the key difference between ISORS and the focus-matched ISORS, in that for traditional ISORS ballistic photons do not impinge on the optical axis within the medium, as shown in Fig. 1(b) (I). In order for focus-matched ISORS to provide an improvement over traditional ISORS, the optical penetration depth of the medium must be sufficiently high that a tightly-focused spot can be formed near the center of the container by ballistic photons. This is why there is no marked difference between the ISORS geometries for highly scattering media, while the focus-matched configuration provides an additional signal boost in weakly scattering media.

We note in passing that, for the highly scattering case, a slight boost in contents signal can still be achieved when compared to traditional ISORS, if the collection and excitation focal depth are carefully selected. Even at high scattering, there is still a peaked intensity distribution along the beam axis (see Fig. 4). As shown in Figure S4, we have established an empirical relationship between the optical penetration depth of the medium and the 1/e point of this intensity peak. In an experiment, there is therefore still some boost to the contents signal possible by restricting the focal points of collection and excitation to account for the optical penetration depth of the sample.

For illustrative clarity, we have given the above demonstration for a flat container. In many samples of interest, containers will have curved surfaces, which will create astigmatism or other aberrations in the beam. However, for typical glass bottles, this astigmatism does not prevent the focus-matched ISORS approach from improving the signal and contents-container ratio, as demonstrated in Figure S5.

3.3. Optimizing focus-matched ISORS

The set-up in Fig. 1(c) was used to study the same whisky samples in an optimized focus-matched ISORS configuration. In order to achieve the best surface suppression effect and signal intensity, a judicious choice of lenses can be made.

Most obvious of these is that the lens L_{2b} should be chosen with the highest possible numerical aperture (shortest focal length) to optimize the signal collection, as shown in Fig. 5(a) (green points). However, high numerical aperture optics often require a compromise in the focal length. Figure 5(b) shows that for the 70mm glass bottles, the best container-to-contents ratio is obtained by collecting from deeper inside the bottle. This is because the glass signal is increasingly suppressed by increasing the spatial separation between the collection focal point and the surface of the bottle (Fig. 5(a)). The trade-off between these requirements can be seen more clearly for smaller bottles such as the example in Fig. 5(d) and Fig. 5(e), which has a 35 mm diameter. Setting the collection point near the center of the container gives the minimum container-to-contents ratio (Fig. 5(e)). This is because maximizing the offset distance from any glass surface minimizes its contribution to the total signal (Fig. 5(d)), and moving the collection point beyond the center of the bottle causes signal from the back surface of the container to be detected (which we verified in our MCRT model, Figure S6). Combining the optimal glass suppression distance with the requirement for highest signal collection efficiency, we see that the optimal focal length of L_{2b} allows collection from the approximate center of the bottle.

Increasing the focal length of L_{1b} increases the demagnification of the Bessel beam produced by the axicon. This minimizes the size of excitation spot, producing a high intensity and thus high signal from the contents. This also increases the size of the ring entering L_{2b}, and thus the ring size on the bottle surface, reducing the signal from the container which is collected by the fiber. The ratio L_{3b} / L_{2b} can be chosen to maximize the collection of the contents signal while

Optics EXPRESS

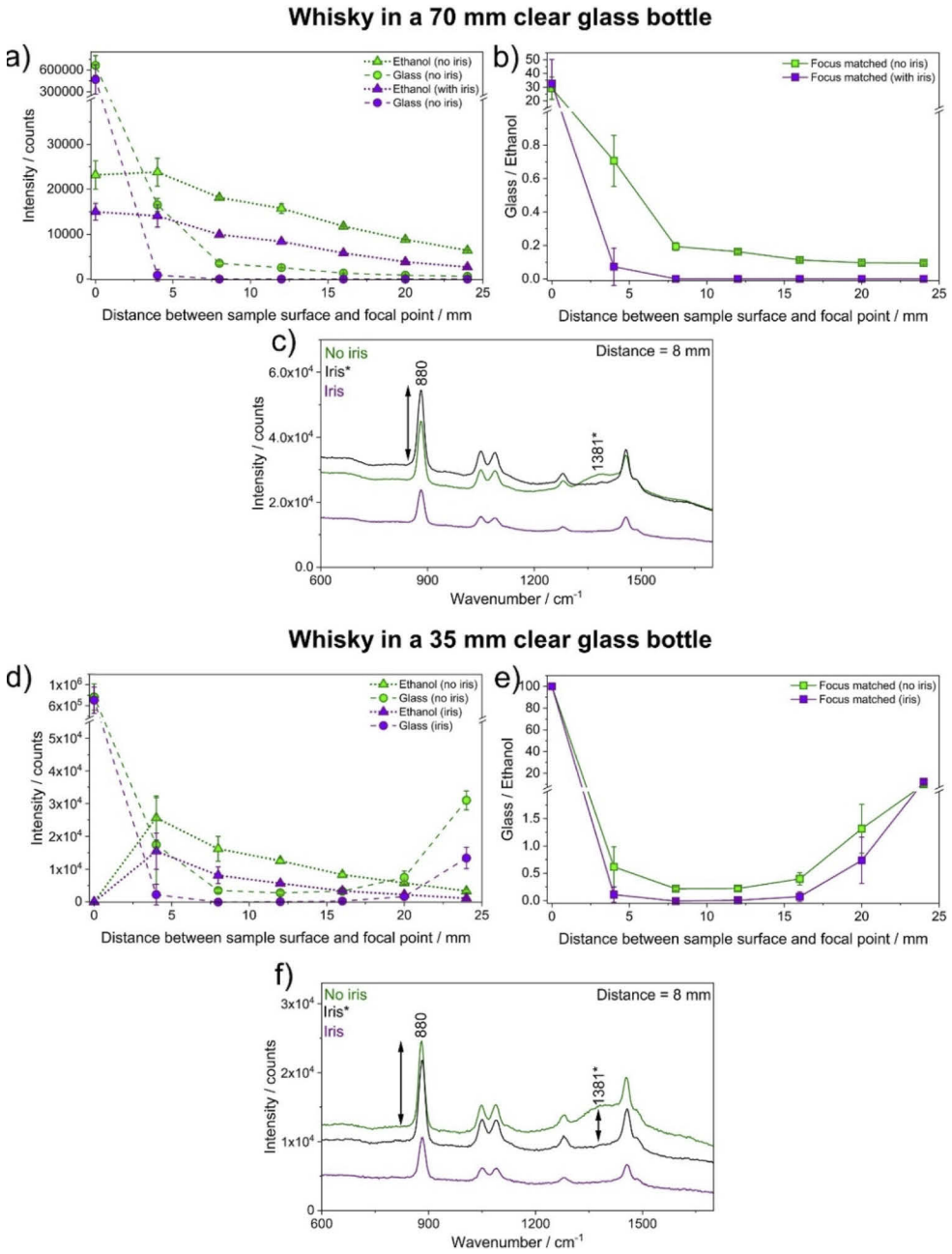

Fig. 5. Variation of Raman spectra in the exclusively focus-matched configuration (Fig. 1(c)), for whisky in (a-c) 70 mm and (d-f) 35 mm clear glass bottles, as a function of distance between the sample surface and the focal point of L_{2b}. Here, the glass signal can be excluded in entirety whilst maintaining a strong signal intensity of the contents. a) and d) Intensities of the respective glass (1381 cm^{-1}) and ethanol (880 cm^{-1}) bands, with (purple) and without (green) inclusion of an iris. b) and e) Container-to-contents ratios obtained with (purple) and without (green) inclusion of an iris in the setup. c) and f) Spectra obtained at their lowest container-to-contents ratio with container peaks labelled with an *. The black spectrum* is obtained with an iris but with an increased CCD slit width to improve signal intensity. Arrows indicate method of measurement of peak heights.

Optics EXPRESS

simultaneously ensuring that the signal from the glass surface misses the fiber front facet, as demonstrated in Figure S7.

Figure S1 shows the suppression effect on a whisky sample for four different combinations of lenses with varying focal lengths. For 70 mm-diameter glass bottles, we find an optimal combination of focal lengths to be L_{1b} = 100 mm, L_{2b} = 40 mm, L_{3b} = 50 mm. This is consistent with the logic outlined in the preceding paragraphs: f = 100 mm is the longest focal length we tested for L_{1b}; for L_{2b}, f = 40 mm is close to the bottle radius (35 mm); and a magnification of 1.2x in the L_{2b}-L_{3b} combination gives the best compromise between collection efficiency of contents signal and suppression of container signal at the front facet of our spectrometer collection fiber.

In our previous work [21] it was noted that inclusion of an iris aperture functioned to further exclude fluorescence signal from the glass bottle, whilst selectively retaining signal from the alcohol contents. In the optimized focus-matched geometry, the role of the iris aperture was explored in more detail (purple points in Fig. 5). In the case of the 70 mm diameter whisky bottle in Fig. 5(a), inclusion of the iris considerably improves the glass suppression effect over a broad range of ring sizes, such that a minimal container-to-contents is achieved for a larger range of bottle positions (Fig. 5(b)), as long as the Bessel beam is formed inside the approximate middle region of the sample. In fact, as illustrated in Fig. 5(c) and 5(e), inclusion of an iris can suppress the glass signal completely. The resulting spectra obtained are free of the glass signal and almost exactly match that obtained from the same whisky sample measured inside a quartz cuvette (Figure S8). The glass-to-ethanol ratio therefore reaches zero when no glass signal is observed.

We note that the optimal position for an iris would intuitively be on an image plane of the excitation focus and thereby realizing a confocal pinhole geometry, which is well known to exclude out-of-plane light. However, given the high degree of extinction demonstrated without this positioning for the case of the whisky bottles, in the interest of simplicity we have elected not to add the extra elements required to realize this additional image plane. Inclusion of the iris does decrease the overall signal intensity; however, the spectra are still of good quality and can be further improved by increasing the size of the entrance slit to the CCD (black points in Figs. 5(c) and 5(f)). We find that an aperture diameter of around 10 mm is a good compromise between signal level and glass suppression: smaller apertures significantly reduce the total signal without further improving the container-to-contents ratio (Figure S9). This focus-matched configuration, combined with an iris aperture, allows for the acquisition of container-free spectra of a glass bottle's contents without the need for the typical scaled spectral subtraction performed in traditional ISORS.

4. Conclusion

In the case of weakly scattering media, adoption of a focus-matched ISORS configuration where the excitation and collection foci overlap presents several advantages over the conventional ISORS set-up. Namely, the ability of photons to penetrate ballistically deep inside the sample, and therefore form a tight focus, leads to an increased generation of Raman scattered photons from the contents. This significantly boosts the signal of contents relative to that of the container. Furthermore, photons collected from the container can be further suppressed by inclusion of an iris aperture in the system. In the case of whisky in a clear glass bottle, we have demonstrated that the utilization of this method allows the fluorescence signal of the glass to be bypassed entirely, facilitating acquisition of isolated Raman spectra of the contents, without the need for spectral subtraction. Larger diameter bottles allow more flexibility in the sample's positioning, due to reduced contribution from the back glass wall.

The focus-matched configuration does not hold any notable advantages for highly scattering media, such as opaque plastic and paracetamol tablets, due to the limited penetration depth. However, importantly, offsetting the collection focus beyond that of the sample's surface can help to reduce signal attributed to the container [10,11]. As with traditional ISORS, barrier

Optics EXPRESS

materials with exceptionally high absorption or strong fluorescence will continue to prevent sample interrogation.

In order to optimize the choice of optical components in a focus-matched ISORS configuration, the size, shape and optical properties of the sample under investigation all play a role. In general, the collection point should be as far from the container walls as possible to maximize the suppression of container signals, but no larger than the optical penetration depth in order to retain a high contents signal. While respecting this constraint, a higher numerical aperture of the combined excitation / collection lens will serve to maximize the size of the ring on the bottle surface, which improves the suppression of the container, and to maximize collection of contents signal. The magnification of the system which images the collection plane onto the spectrometer input can be increased to minimize the collection of container signal, but only up to a value which allows all the contents light to still be collected on the detector. The inclusion of an iris in the detection path can also serve to remove container signal. For a typical 70 mm diameter whisky bottle and a collection fiber with 200 µm core diameter, an empirical optimization of 25.4 mm-diameter optical components led to a system comprising an $f = 40$ mm collection lens, an imaging telescope with 1.2x magnification and an iris diameter of 10 mm.

In conclusion, we have shown that when designing an offset Raman spectroscopic probe for samples inside containers, one should pay careful attention to the scattering and absorption properties of the container and the medium, in order to optimally detect the contents while minimizing signal from the container. When the optical penetration depth of the sample is larger than or approximately equal to the depth at which the sample is probed, the tightly-focused beam produced in the focus-matched ISORS configuration will offer an enhancement of the signal of the contents while maintaining the container extinction properties of traditional ISORS. For example, the signal of the contents for whisky in original glass containers is enhanced by a factor of 3 in both signal strength and signal to noise ratio. The focus-matched geometry should prove to be particularly useful for anti-counterfeiting and adulterant detection of liquids, and has the potential to function as a compact, portable device.

Funding. Engineering and Physical Sciences Research Council (EP/P030017/1, EP/R004854/1); Horizon 2020 Framework Programme (EC-GA 863203).

Acknowledgements. The authors thank Mingzhou Chen for useful discussions and Rory M. Bruce for the loan of Lego used in this study

Disclosures. The authors declare that there are no conflicts of interest related to this article

Data availability. The research data supporting this publication can be accessed at Ref. [31].

Supplemental document. See Supplement 1 for supporting content.

References

1. C. Eliasson, N. A. Macleod, and P. Matousek, "Non-invasive detection of cocaine dissolved in beverages using displaced Raman spectroscopy," Anal. Chim. Acta **607**(1), 50–53 (2008).
2. F. Nicolson, L. E. Jamieson, S. Mabbott, N. C. Shand, D. Graham, and K. Faulds, "Through barrier detection of ethanol using handheld Raman spectroscopy—Conventional Raman versus spatially offset Raman spectroscopy (SORS)," J. Raman Spectrosc. **48**(12), 1828–1838 (2017).
3. J. Kiefer and A. L. Cromwell, "Analysis of single malt Scotch whisky using Raman spectroscopy," Anal. Methods **9**(3), 511–518 (2017).
4. P. Buzzini and E. Suzuki, "Forensic applications of Raman spectroscopy for the in situ analyses of pigments and dyes in ink and paint evidence," J. Raman Spectrosc. **47**(1), 16–27 (2016).
5. J. C. Carter, W. E. Brewer, and S. M. Angel, "Raman spectroscopy for the in situ identification of cocaine and selected adulterants," Appl. Spectrosc. **54**(12), 1876–1881 (2000).
6. S. Gulia, K. K. Gulati, V. Gambhir, and R. Sharma, "Detection of explosive materials and their precursors through translucent commercial bottles using spatially offset Raman spectroscopy using excitation wavelength in visible range," Opt. Eng. **58**(12), 1 (2019).
7. B. Zachhuber, C. Gasser, E. t. Chrysostom, and B. Lendl, "Stand-off spatial offset Raman spectroscopy for the detection of concealed content in distant objects," Anal. Chem. **83**(24), 9438–9442 (2011).

Optics EXPRESS

8. P. Matousek, I. P. Clark, E. R. C. Draper, M. D. Morris, A. E. Goodship, N. Everall, M. Towrie, W. F. Finney, and A. W. Parker, "Subsurface probing in diffusely scattering media using spatially offset Raman spectroscopy," Appl. Spectrosc. **59**(4), 393–400 (2005).
9. S. Mosca, C. Conti, N. Stone, and P. Matousek, "Spatially offset Raman spectroscopy," Nat. Rev. Methods Primers **1**(1), 21 (2021).
10. M. D. Hargreaves and P. Matousek, "Threat detection of liquid explosive precursor mixtures by Spatially Offset Raman Spectroscopy (SORS)," Proc. SPIE **74860**, 74860B (2009).
11. C. Eliasson, N. A. Macleod, and P. Matousek, "Noninvasive detection of concealed liquid explosives using Raman spectroscopy," Anal. Chem. **79**(21), 8185–8189 (2007).
12. D. I. Ellis, R. Eccles, Y. Xu, J. Griffen, H. Muhamadali, P. Matousek, I. Goodall, and R. Goodacre, "Through-container, extremely low concentration detection of multiple chemical markers of counterfeit alcohol using a handheld SORS device," Sci. Rep. **7**(1), 12082 (2017).
13. D. I. Ellis, H. Muhamadali, Y. Xu, R. Eccles, I. Goodall, and R. Goodacre, "Rapid through-container detection of fake spirits and methanol quantification with handheld Raman spectroscopy," Analyst **144**(1), 324–330 (2019).
14. C. Eliasson, M. Claybourn, and P. Matousek, "Deep subsurface Raman spectroscopy of turbid media by a defocused collection system," Appl. Spectrosc. **61**(10), 1123–1127 (2007).
15. C. Eliasson and P. Matousek, "Noninvasive authentication of pharmaceutical products through packaging using spatially offset Raman spectroscopy," Anal. Chem. **79**(4), 1696–1701 (2007).
16. P. Matousek and N. Stone, "Development of deep subsurface Raman spectroscopy for medical diagnosis and disease monitoring," Chem. Soc. Rev. **45**(7), 1794–1802 (2016).
17. P. Matousek, "Inverse spatially offset Raman spectroscopy for deep noninvasive probing of turbid media," Appl. Spectrosc. **60**(11), 1341–1347 (2006).
18. K. M. Khan, S. B. Dutta, N. Kumar, A. Dalal, A. Srivastava, H. Krishna, and S. K. Majumder, "Inverse spatially-offset Raman spectroscopy using optical fibers: An axicon lens-free approach," J. Biophotonics **12**(11), e201900140 (2019).
19. W. J. Olds, E. Jaatinen, P. Fredericks, B. Cletus, H. Panayiotou, and E. L. Izake, "Spatially offset Raman spectroscopy (SORS) for the analysis and detection of packaged pharmaceuticals and concealed drugs," Forensic Sci. Int. **212**(1-3), 69–77 (2011).
20. K. M. Khan, S. B. Dutta, H. Krishna, and S. K. Majumder, "Inverse SORS for detecting a low Raman-active turbid sample placed inside a highly Raman-active diffusely scattering matrix – A feasibility study," J. Biophotonics **9**(9), 879–887 (2016).
21. H. Fleming, M. Chen, G. D. Bruce, and K. Dholakia, "Through-bottle whisky sensing and classification using Raman spectroscopy in an axicon-based backscattering configuration," Anal. Methods **12**(37), 4572–4578 (2020).
22. I. R. M. Barnard, P. Tierney, C. L. Campbell, L. McMillan, H. Moseley, E. Eadie, C. T. A. Brown, and K. Wood, "Quantifying Direct DNA Damage in the Basal Layer of Skin Exposed to UV Radiation from Sunbeds," Photochem. Photobiol. **94**(5), 1017–1025 (2018).
23. L. McMillan, S. Reidt, C. McNicol, I. R. Barnard, M. MacDonald, C. T. Brown, and K. Wood, "Imaging in thick samples, a phased Monte Carlo radiation transfer algorithm," J. Biomed. Opt. **26**(09), 096004 (2021).
24. K. Wood and R. J. Reynolds, "A Model for the Scattered Light Contribution and Polarization of the Diffuse Hα Galactic Background," Astrophys. J. **525**(2), 799–807 (1999).
25. R. L. McCreery, *Raman Spectroscopy for Chemical Analysis* (John Wiley & Sons, 2000), Chap. 4.
26. F. Menges, "Spectragryph - optical spectroscopy software", Version 1.2.14, (2021).
27. L. McMillan, G. D. Bruce, and K. Dholakia, "Meshless Monte Carlo Radiation Transfer Method for Curved Geometries using Signed Distance Functions," https://arxiv.org/abs/2112.08035
28. J. R. Maher and A. J. Berger, "Determination of Ideal Offset for Spatially Offset Raman Spectroscopy," Appl. Spectrosc. **64**(1), 61–65 (2010).
29. D. Toublanc, "Henyey–Greenstein and Mie phase functions in Monte Carlo radiative transfer computations," Appl. Opt. **35**(18), 3270–3274 (1996).
30. S. Jacques, R. Joseph, and G. Gofstein, "How photobleaching affects dosimetry and fluorescence monitoring of PDT in turbid media," Proc. SPIE **1881**, 168–179 (1993).
31. G. E. Shillito, L. McMillan, G. D. Bruce, and K. Dholakia, "Data Underpinning To focus-match or not to focus-match inverse spatially offset Raman spectroscopy: a question of light penetration," University of St Andrews Research Portal (2022).https://doi.org/10.17630/6afe39e2-5988-4c87-bf8a-d6228593364cS